Supplementary Materials

Direct visualization of percolating metal-insulator transition in V_2O_3 using scanning microwave impedance microscopy

Weiyan Lin[1], Huanyu Zhang[2], Yoav Kalcheim[3,4], Xinchen Zhou[2,5], Fubao Yang[2,5], Yang Shi[1], Yang Feng[2,6], Yihua Wang[2,7], Jiping Huang[2,5], Ivan K. Schuller[3,4],

Xiaodong Zhou[1,9,10]†, and Jian Shen[1,2,7,8,9,10]†

[1]State Key Laboratory of Surface Physics and Institute for Nanoelectronic Devices and Quantum Computing, Fudan University, Shanghai, China.
[2]Department of Physics, Fudan University, Shanghai, China.
[3]Department of Physics, University of California San Diego, La Jolla, California 92093, USA
[4]Center for Advanced Nanoscience, University of California San Diego, La Jolla, California 92093, USA
[5]Key Laboratory of Micro and Nano Photonic Structures (MOE), Fudan University, Shanghai, China
[6]Beijing Academy of Quantum Information Science, Beijing, China
[7]Shanghai Research Center for Quantum Sciences, Shanghai, China.
[8]Collaborative Innovation Center of Advanced Microstructures, Nanjing, China
[9]Shanghai Qi Zhi Institute, Shanghai, China
[10]Zhangjiang Fudan International Innovation Center, Fudan University, Shanghai, China

†Emails: zhouxd@fudan.edu.cn, shenj5494@fudan.edu.cn

Contents:

Figure S1 to S9

SI A: Finite element analysis simulation of scanning Microwave Impedance Microscopy signal

To better understand the dependence of scanning microwave impedance microscopy (sMIM) signal on sample's local conductivity, we perform a finite element analysis (FEA) simulation of the tip-sample admittance *Y* using a commercial software COMSOL. The sMM signal is proportional to such an admittance. For a two-dimensional thin film, we use a sheet resistance (Ω /□) to represent its conductivity. In the simulation, we construct a tip-sample interface with some given material/geometric parameters. In particular, we set the radius of the tip as 50 nm, the thickness of V_2O_3 thin film as 300 nm, and the dielectric constant of V_2O_3 (Al_2O_3 substrate) as 4 (9). We then vary the sheet resistance of V_2O_3 and calculate the corresponding tip-sample admittance in order to obtain a so-called sMIM response curve as shown in the Fig. S1. While the sMIM-Im signal decreases monotonically with the increasing sheet resistance, the sMIM-Re signal exhibits a peak as a function of the sheet resistance. Another important information from our simulation is the penetration depth of the sMIM signal into the V_2O_3 thin film. The inset of Fig. S1 shows the simulated quasi-static potential around the tip which can be used to estimate the penetration depth of the applied microwave signal. The simulation was done for a typical sheet resistance of 10^4 Ω. The microwave signal clearly penetrates into the whole 300 nm V_2O_3 thin film. In other words, it can sense the electric property of the whole film which makes sMIM very powerful as compared to other surface sensitive probes. Moreover, the lateral spatial resolution of sMIM is largely determined by the tip radius which is roughly 100 nm in our case.

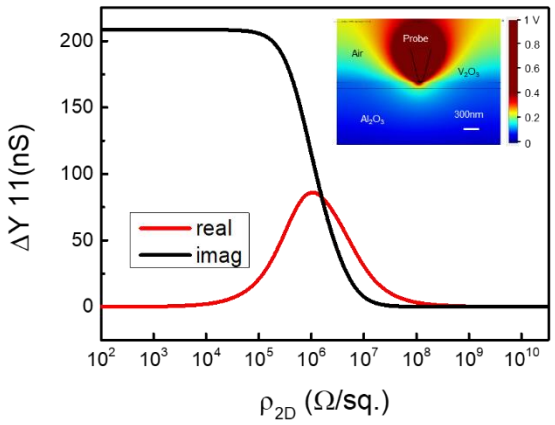

FIG S1 FEA simulation of the sMIM response curve and the quasi-static potential at the tip-sample interface.

SI B: sMIM image data normalization

The raw sMIM image data has a temperature dependent signal background. It will change with the temperature as the length of the microwave circuit components changes due to the

thermal expansion. We perform the temperature dependent sMIM imaging in V_2O_3 to monitor its metal-insulator transition (MIT). To make the sMIM images taken at various temperatures directly comparable, this temperature dependent signal shift has to be compensated. In practice, we use a gold metal electrode as a temperature independent normalization reference. The sMIM signal will saturate at the gold electrode due to its very large conductivity, which thus doesn't have a temperature dependence. For each raw sMIM image, we include the gold metal electrode in the scan field of view, and subtract sMIM signal on gold from signals taken on sample areas. After the subtraction, the normalized sMIM images are comparable as they share the same high limit and only reflect the relative change of conductivity between metallic and insulating phases. Figure S2 (a) shows an optical image of our V_2O_3 device with the sMIM scan field of view marked by the red rectangle. Figure S2(b) and (c) are simultaneously taken AFM topography and sMIM-Im images at 164 K with the gold electrode on the left. The sMIM-Im signal has been normalized, so the gold electrode signal is 0 representing the most conductive part. The metallic phases in V_2O_3 show almost the same signal level with the gold with a clear image contrast with the insulating phases. Please note that we don't include the gold in sMIM images shown in the main text.

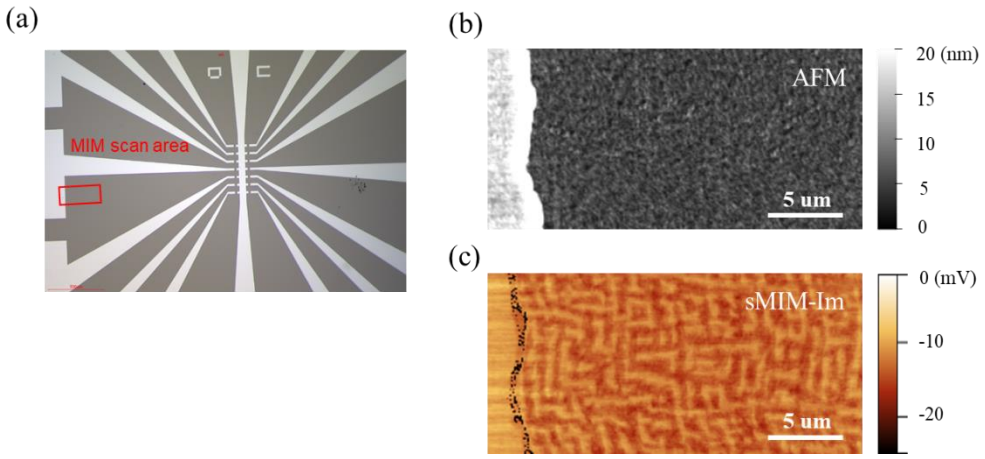

FIG S2 (a) Optical image of V_2O_3 device with the lithographically defined meal electrodes. (b) AFM topography of the V_2O_3. (c) The normalized sMIM-Im image of the V_2O_3. Scale bar is 5 μm.

SI C: The irrelevance of topography to the electronic domain pattern

To study the correlation between electronic domain pattern and the topography, we follow exactly the same procedure as was done in Ref. 16 of the main text to analyze our data. Figure S3 show the topographic images taken at 200 K (far away from MIT) and 164 K (in the middle of MIT) on the same area, as well as a simultaneously taken sMIM image at 164 K showing a bi-directional striped domain pattern. By subtracting topography at 200 K from the one at 164 K, we obtain the difference in topographic height in Fig. S3(d) which doesn't show the striped pattern as sMIM image in Fig. S3(b). Therefore, the topography is irrelevant to the electronic domain pattern revealed from the sMIM imaging.

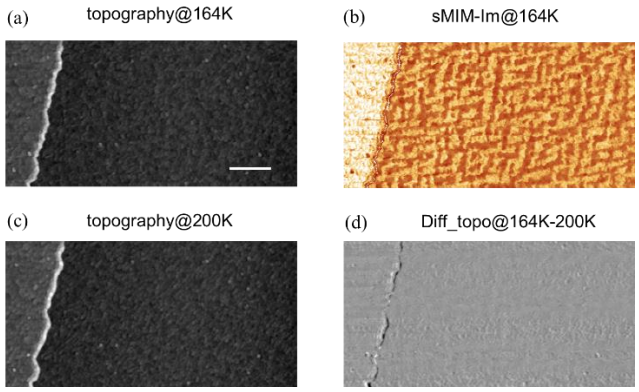

FIG S3 (a) The AFM topographic image of V_2O_3 taken at 164 K. Scale bar is 5 μm. (b) Simultaneously taken sMIM image with Fig. S3(a). A bi-directional striped pattern can be seen. (b) The AFM topographic image from the same area as Fig. S3(a) taken at 200 K. (d) Difference in topographic height obtained by subtraction of panel (c) from panel (a).

SI D: sMIM imaging of MIT on another sample area

To demonstrate the repeatability of thermal hysteretic behavior in the domain evolution, we show sMIM imaging data taken on another sample area. Similar to Fig. 1(b), one sees a continuous domain growth procedure with percolating characters (Fig. S4(a)). A thermal hysteresis is directly resolved as well, i.e., one reaches the same metallic phase fraction at a higher temperature in the warming than that in the cooling. Figure S4(b) is the extracted metallic phase fraction as a function of the temperature $p(T)$. Such $p(T)$ shows a slope change when $p \sim$ 50% signaling a percolation process. In addition, the thermal hysteresis of $p(T)$ is larger at lower temperatures and shrinks at higher temperatures reconfirming an important observation we have in the main text, i.e., cooling and warming represent two different percolating processes.

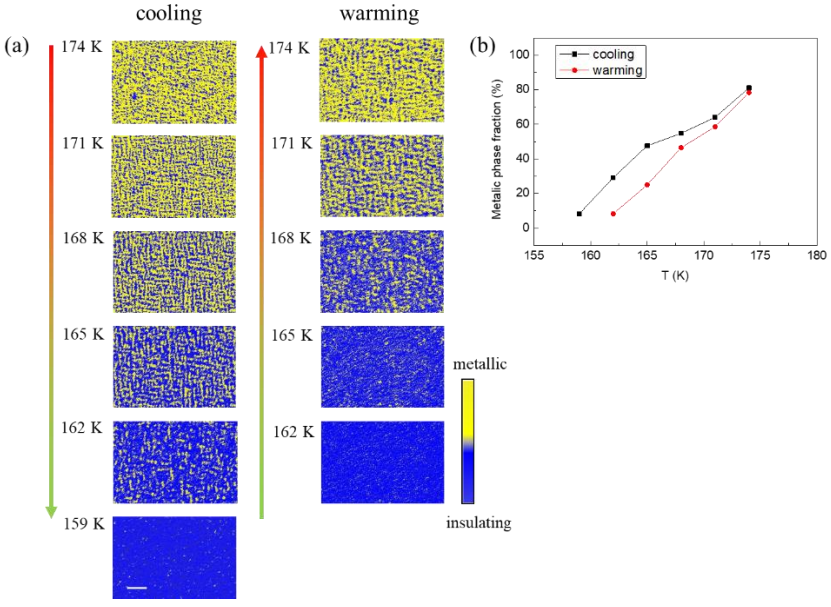

FIG S4 (a) Temperature dependent sMIM images for a cooling and warming cycle of MIT. Scale

bar is 5 μm.. (b) Temperature dependent metallic phase fraction.

SI E: Domain identification and growth simulation

To reveal the difference in domain growth between cooling and warming, we take a closer look at sMIM images. Figure S5(a) and (d) show sMIM images of cooling (173 K) and warming (164 K) process, respectively. They are chosen because they possess a similar minority phase area fraction. However, the minority phase (metallic phase) of warming looks much more fragmented than that (insulating phase) of cooling. In other words, the averaged domain size of the metallic phase in the warming is smaller than that of insulating phase in the cooling. To better quantify this contrasting behavior, we apply an algorism to identify the domains and/or nucleation sites in the sMIM image. Such determination is straightforward. We first binarize every pixel of the image to be either "metallic" or "insulating". Then we look for a cluster of interconnected image pixels of the minority phase, which is metallic (insulating) phase for warming (cooling). Such a cluster has to be enclosed by the majority phase, then is counted as one domain and/or nucleation site. The actual pixel number in one such cluster can vary from one to many depending on the size of the cluster. However, there is an uncertainty of this domain identification mainly from the image pixel binarization, scanning spike noise or topographic artifacts. We adopt two ways to mitigate such an uncertainty in our algorism. First, we set a lower bound of the cluster size. For example, we throw out cluster that has only one pixel which is strongly influenced by the factors mentioned above. We can also raise the bound to 2, 3 or 4 pixels. Second, we require that all the identified domain and/or nucleation sites should be in a "growth mode". For that purpose, we carefully compare the minority phase domain positions in two consecutive sMIM images in the warming and cooling by overlapping them. Figure S5 (b) and (e) show overlapped 173 K and 170 K (164 K and 167 K) images for the cooling (warming). Take warming (Fig. S5(e)) as an example. In such an overlapped image, white areas are the insulating phases existing in both temperatures. Black areas correspond to positions identified as metallic domains in both temperatures. The blue areas are metallic phases lost at higher temperature (they only exist at 164 K, but disappear at 167 K). Now we only keep the domains in the "growth mode" and throw out ones that are not, i.e., we only count the metallic domains that have an overlap with its counterparts at higher temperatures and remove the ones that disappear at higher temperatures. One can see from Fig. S5(e) that most of such left domains (black) indeed expand into larger ones (red) at higher temperatures. The same criterion applies to cooling as well. Figure S5 (c) and (f) show the positions of the identified domains and/or nucleation sites for the cooling and warming, respectively. After all the domains and/or nucleation sites are determined, we get the number for each sMIM image with a certain minority phase area fraction. We plot such number versus area fraction in Fig. 4(a) of the main text. The error bar shown in Fig. 4(a) of the main text comes from the different lower bounds of domain size we tried in the algorism from 2 to 5. The overall behavior indicates that one has more domains and/or nucleation sites in the warming than that of cooling at the beginning of domain growth.

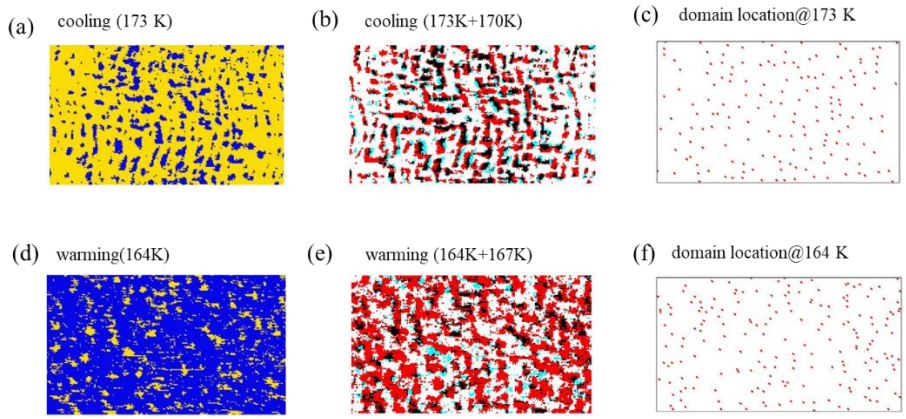

FIG S5 (a) sMIM images at 173 K of cooling. (b) overlapped sMIM images at 173 K and 170 K of cooling. (c) domain position identification for cooling. (d) sMIM images at 164 K of warming. (e) overlapped sMIM images at 164 K and 167 K of warming. (f) domain position identification for warming.

We apply a random-resistor network model to simulate the domain growth as well as calculate the macroscopic conductance of the system. In particular, we adopt a site percolation model in a two-dimensional square lattice as shown in Fig. S6 in which it has two structural elements, a site and a bond. Note that in our simulation, we consider the phase competition of two phases at each spatial location. In other words, the minority phase domain growth happens as a net result of area gained and lost. We get a glimpse of this behavior from Fig. S5(b)(e). To simulate the domain growth (take warming as an example) in such a square lattice model, we adopt a procedure derived from a nearest-neighbor bond correlation model[1]. We use a random normalized value r, which is between 0 and 1, to reflect the metallicity of a bond and a site. To start the simulation, we randomly pick n grid sites representing the nucleation site. These sites are assigned the value 1. Then two site numbers associated with a bond were averaged resulting in a new set of value r'. Then every bond was assigned the corresponding value r'. Next, the four bond numbers associated with a particular site were averaged resulting in a new set of value r''. Every site was assigned the corresponding value r''. This process can be iterated many times. It can make all the nodes around a node of large value grow. Therefore, it can be used to simulate domain growth process. We define the following rules of value assignment: every site was assigned the value r=0.25*(r_1+r_2+r_3+r_4) and every bond was assigned the value r=p*(r_1+r_2) where the coefficient p is chosen 0.55 for simulating the metallic domain growth and 0.45 for the metallic domain lost. To guarantee the net metallic domain growth as seen in the experiment, the probability of bond value assignment choosing p=0.55 (p=0.45) is 53% (47%) among all the bonds at each step of the simulation.

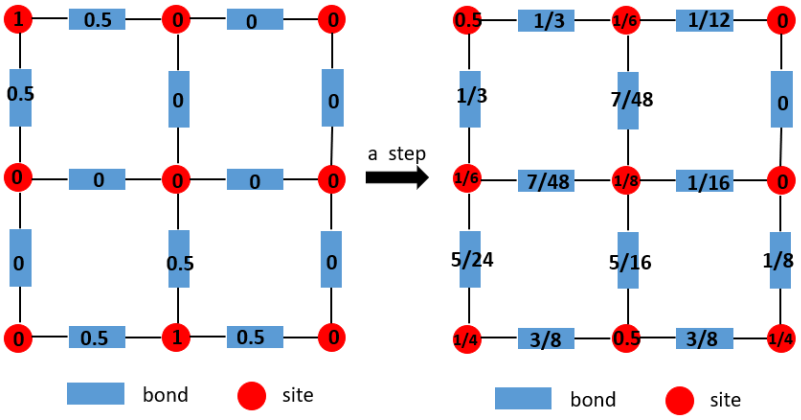

FIG S6 The schematic of nearest-neighbor bond correlation model.

We choose 1000 × 1000 square lattice. Periodic boundary conditions are imposed by connecting pairs of grid points on the opposite free edges. As described above, we randomly pick *n* nucleation site and let the procedure flow. Figure S6 gives an example of value assignment to the bond and site in the model and new values generated in next step. We iterate the procedure 1000 times after which the "minority phase" reaches 100%. In each step, we identify the site whose *r* value is larger (smaller) than 0.5 to be metallic (insulating) so as to get the metallic phase fraction. We also note that, the initially chosen nucleation site number *n* is critical to the observed difference between warming and cooling. Fig. S7 lists four examples of the simulated metallic phase fraction versus simulation steps with different number ratio of initial nucleation site between warming and cooling. When such number is the same, the simulated curves are symmetric in the sense that they overlap after a lateral shift in steps. Increasing the number ratio results in an increasing asymmetry of the line shape, i.e., the curves cannot overlap each other after a lateral shift. We choose 5:1 to generate the simulation shown in Fig. 4(b) in the main text.

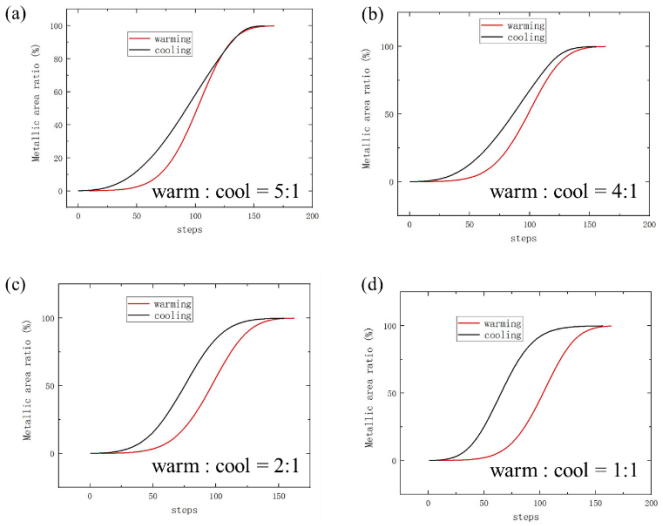

FIG S7 (a-d) Metallic phase fraction as a function of simulation steps under different number ratios of initial nucleation site between warming and cooling.

SI F: Global conductance calculation from random-resistor network model

Given the simulated domain configuration, we can calculate the macroscopic conductance of such random-resistor network model. Figure S8 shows a schematic of the model. Each site *i* (*i* = 1,2,….N) of the lattice is selected as metallic (insulating) as denoted by a filled orange (blue) circle in Fig. S8. Such assignment directly comes from our simulated domain configuration. The conductance of a bond G_{ij} that connects site *i* to site *j* is determined as the followings: 1) if both sites of a bond are insulating, $G_{ij} = G_i$; 2) if both sites of a bond are metallic, $G_{ij} = G_m$; 3) if a bond connects a metallic site to an insulating site, $G_{ij} = 2G_iG_m / \left(G_i + G_m\right)$. Here G_i and G_m are the conductance of metallic and insulating phases during the MIT. We approximate the conductance $G_m = 1$ and $G_i = 0.001$ as a constant value. We also include a source and a sink in the lattice model as denoted by the filled green and red circle in Fig. S8. They are connected to the left and right side of the lattice mimicking the electrode contacts in real transport measurement. We rely on the Kirchhoff's equations to calculate the effective conductance of such resistor network. Kirchhoff's first law leads to the following constraint

$$\sum_{i=1}^{N} I_i = 0$$

Kirchhoff's second law gives rise to

$$\sum_{j=1,\, j\neq i}^{N} G_{ij}\left(V_i - V_j\right) = I_i, i = 1,2,...N$$

where V_i is the electric potential at site *i*. This equation can be rewritten as

$$LV = I$$

where $L = \begin{bmatrix} G_1 & -G_{12} & \cdots & -G_{1,N} \\ -G_{21} & G_2 & \cdots & -G_{2,N} \\ \vdots & \vdots & \ddots & \vdots \\ -G_{N-1,1} & -G_{N-1,2} & \cdots & G_N \end{bmatrix}$, $G_i = \sum_{j=1,\, j\neq i}^{N} G_{ij}$

Here **V** and **I** are N-vectors whose components are V_i and I_i, respectively. Knowing **I** as the boundary condition (a certain amount of current flows from the source to the sink), it is easy to get **V** by dividing **I** by **L**. However, **L** is a singular matrix due to the fact that the zero point of electric potential is not unique which makes the above equation have an infinite number of solutions. To solve this issue, we assign $V_N = 0$. Therefore, **L** can be reduced to

$$L = \begin{bmatrix} G_1 & -G_{12} & \cdots & -G_{1,N-1} \\ -G_{21} & G_2 & \cdots & -G_{2,N-1} \\ \vdots & \vdots & \ddots & \vdots \\ -G_{N-1,1} & -G_{N-1,2} & \cdots & G_{N-1} \end{bmatrix}$$

Now **L** is not a singular matrix. By solving the Kirchhoff's equations listed above, one can get the effective conductance of the random-resistor network.

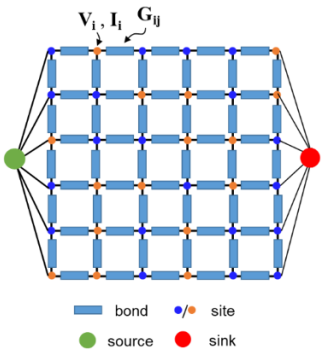

FIG S8 The schematic of our random-resistor network model.

SI G: Comparison of domain distribution above the percolation threshold

To understand the conductance difference between cooling and warming with the same metallic phase fraction, namely the thermal hysteresis in $G(p)$, in the regime above the percolation threshold, we compare sMIM images of cooling and warming with $p \sim 80\%$ as shown below in Fig. S9. The extracted averaged sMIM signal level of metallic (insulating) phases is -13 (-32) mV for the cooling and -12 (-31) mV for the warming meaning the actual mesoscopic conductance of the metallic (insulating) phases vary little between cooling and warming. However, the spatial domain configuration differs. The insulating domain distribution, now as a barrier to the current flow, is more fragmented in the cooling than that of the warming. It may explain why cooling is more conductive than warming even under the same metallic phase fraction because the electric current has a better chance in the cooling to go around the insulating barrier. In other words, the thermal hysteresis in $G(p)$ above the percolation threshold is largely due to the different domain configurations. This experiment also demonstrates the importance of knowing actual spatial domain configuration for understanding the global transport behavior.

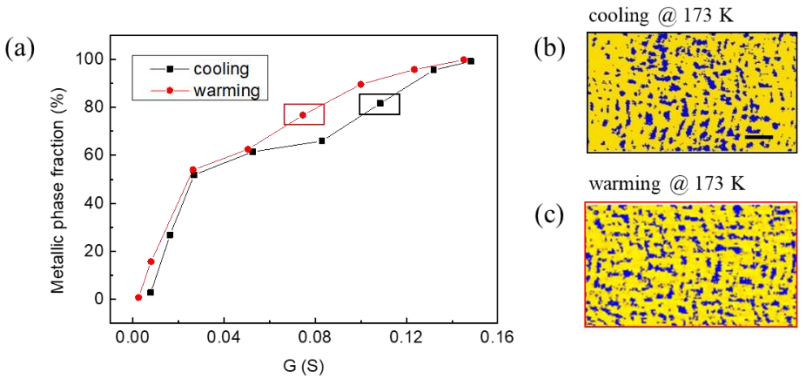

FIG S9 (a) Global conductance versus the metallic phase fraction. (b) sMIM image taken at 173 K in the cooling. Scale bar is 5 μm. (c) sMIM image taken at 173 K in the warming.

References

[1] I. Webman, J. Jortner, and M. H. Cohen, Phys. Rev. B **11**, 2885 (1975).